Nanosecond Dynamics of the Single Tryptophan Reveals Multi-State Equilibrium Unfolding of Protein GB1

Olga Tcherkasskaya,*,‡ Jay R. Knutson,§ Sara A. Bowley,|| M. Kirsten Frank,|| and Angela M. Gronenborn||

Laboratory of Experimental and Computational Biology, National Cancer Institute, National Institutes of Health, Bethesda, Maryland 20892, Laboratory of Cell Biology, National Heart, Lung and Blood Institute, National Institutes of Health, Bethesda, Maryland 20892, and Laboratory of Chemical Physics, National Institute of Diabetes and Digestive and Kidney Diseases, National Institutes of Health, Bethesda, Maryland 20892

Received February 15, 2000; Revised Manuscript Received June 21, 2000

ABSTRACT: Unfolding of the immunoglobulin binding domain B1 of streptococcal protein G (GB1) was induced by guanidine hydrochloride (GdnHCl) and studied by circular dichroism, steady-state, and time-resolved fluorescence spectroscopy. The fluorescence methods employed the single tryptophan residue of GB1 as an intrinsic reporter. While the transitions monitored by circular dichroism and steady-state fluorescence coincided with each other, the transitions followed by dynamic fluorescence were markedly different. Specifically, fluorescence anisotropy data showed that a relaxation spectrum of tryptophan contained a slow motion with relaxation times of 9 ns in the native state and 4 ns in the unfolded state in 6 M GdnHCl. At intermediate GdnHCl concentrations of 3.8−4.2 M, however, the slow relaxation time increased to 18 ns. The fast nanosecond motion had an average time of 0.8 ns and showed no dependence on the formation of native structure. Overall, dynamic fluorescence revealed two preliminary stages in GB1 folding, which are equated with the formation of local structure in the β_3-strand hairpin and the initial collapse. Both stages exist without α-helix formation, i.e., before the appearance of any ordered secondary structure detectable by circular dichroism. Another stage in GB1 folding might exist at very low (∼1 M) GdnHCl concentrations.

Equilibrium unfolding of globular proteins offers insights into various interactions that govern the stability of native structures, and may provide clues to the pathway of folding. Unfolding induced by denaturants is modeled, in many cases, by a two-state mechanism involving the native and the unfolded state (*1, 2*). The native state is considered to comprise an ensemble of molecules, which share a common fold with the unique three-dimensional structure. The unfolded state is thought to be more or less a random coil, with little or no regular structure. The number of reports, however, testifying to the existence of equilibrium and/or kinetic intermediates in (un)folding induced by denaturants, increases steadily. An incomplete list includes β-lactamase (*3*), carbonic anhydrase B (*4*), ribonuclease A (*5*), *E. coli* dihydrofolate reductase (*6*), barstar (*7, 8*), cytochrome *c* (*9*), yeast phosphoglycerate kinase *(10),* and many others (*11*). Although these studies have focused mostly on the "molten globule" state, they also raised new questions with respect to the denatured state. For example: How do we define the unfolded state, and what is the role of local interactions in protein folding? In fact, the local interactions in an unfolded polypeptide chain could guide the protein toward an intermediate conformation, creating folding nuclei, thereby reducing the search through conformational space (*12*). Identifying the existence of folding initiation sites, as well as unfolded or partly folded intermediates, presents a difficult challenge. It depends crucially on the population of intermediate states and requires significant differences in their thermodynamic and kinetic properties. Traditionally, if nearly identical (un)folding curves are observed by experimental measurements characterizing secondary and tertiary structures, a two-state mechanism is assumed (*5, 13*). This congruence, however, cannot be considered as sufficient evidence for a two-state model, especially if folding intermediates have no regular structure. Clearly, the lack of appropriate probes for studying protein folding may contribute to the absence of observable intermediates. In an endeavor to understand protein folding, detailed multiparametric investigations of equilibrium (un)folding are required. Whether equilibrium intermediates are also intermediates on the kinetic folding pathway remains a serious question.

Over the last couple of years, several model systems have emerged which have found widespread use in the protein folding field. One such protein is the immunoglobulin binding domain B1 of streptococcal protein G (GB1).[1] NMR and fluorescence studies on GB1 support the two-state mechanism of folding, suggesting as the initial state of

* To whom correspondence should be addressed. Telephone: (301)-496-9065. Fax: (301)402-4724. E-mail: tcherkasskaya@nih.gov.

‡ Laboratory of Experimental and Computational Biology, National Cancer Institute.

§ Laboratory of Cell Biology, National Heart, Lung and Blood Institute.

|| Laboratory of Chemical Physics, National Institute of Diabetes and Digestive and Kidney Diseases.

[1] Abbreviations: CD, circular dichroism; DAS, decay-associated spectra; GB1, immunoglobulin G-binding domain B1 of streptococcal protein G; GdnHCl, guanidine hydrochloride; NMR, nuclear magnetic resonance.

10.1021/bi000345u
Published on Web 08/16/2000

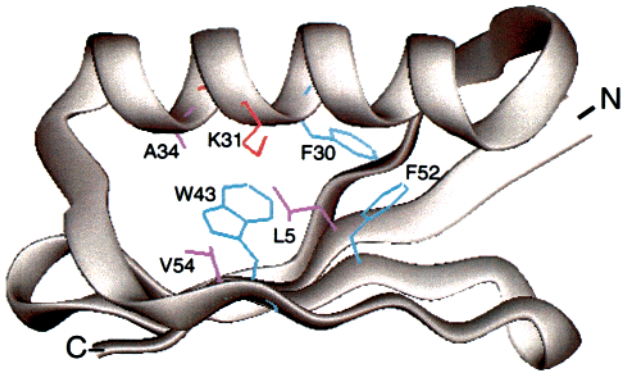

FIGURE 1: Ribbon diagram of the B1 domain of streptococcal protein G. The single tryptophan residue W43 is located on β-strand 3 and is partially buried in the core of the protein. It makes close (<5 Å) hydrophobic contacts with two aromatic (F30, F52) and three aliphatic (L5, A34, V54) residues. Also shown is the positively charged polar side chain of K31.

folding a partly collapsed chain (*14*). Recently, experimental evidence for the presence of an early kinetic folding intermediate containing a native-like core was proposed based on stopped-flow fluorescence measurements (*15*).

GB1 is a small (56 residues), stable, single-domain protein with one α-helix and a four-stranded β-sheet comprised of two hairpins (Figure 1). A single tryptophan residue (W43) is located on β-strand 3, and the local environment of W43 in the native state is mostly hydrophobic. Its side chain is in van der Waals contact (<5 Å) with two aromatic and three aliphatic residues. Thus, W43 is involved in the formation of the interface between the α-helix through contacts with F30 and A34 and the neighboring β-strands through interactions with L5, F52, and V54. Since W43 occupies a critical position in the hydrophobic core of GB1, it constitutes an ideal probe for studying protein folding with time-resolved fluorescence spectroscopy. Dynamic fluorescence measurements are known to be more sensitive to rearrangements of macromolecular structure than steady-state ones (*16*); thus, they may reveal the presence of intermediates more readily, either in equilibrium or in kinetic studies. The present study employs time-resolved fluorescence spectroscopy to follow the equilibrium unfolding transition upon denaturation of GB1 by guanidine hydrochloride (GdnHCl). We demonstrate that it is possible to observe conformations partially structured around W43 which are present under strongly denaturing conditions. These partially folded equilibrium intermediates are likely related to the kinetic folding intermediate reported by Park et al. (*15*).

MATERIALS AND METHODS

Chemicals and Solutions. GB1 was expressed and purified essentially as described previously (*17*). The protein was dissolved in 20 mM sodium phosphate buffer (pH 5.7) containing the desired amount of GdnHCl. Protein concentration was estimated by absorbance using a Hewlett-Packard 8452A diode array spectrophotometer. The molar extinction coefficient at 280 nm was calculated from the tryptophan and tyrosine composition and the standard values of 5690 and 1280 $M^{-1}\cdot cm^{-1}$ reported for those amino acids (*18*, *19*). Ultrapure GdnHCl was purchased from U.S. Biochemicals Inc. and further purified by recrystallization from water and thereafter from ethanol. GdnHCl concentration was determined by refractive index measurements using an AO Abbe refractometer (*20*, *21*). All experiments were carried out at 20 ± 0.05 °C controlled by an RTE-111 Neslab water bath. The pH was measured using a Radiometer PHM83. Experiments were carried out for protein concentrations covering the range of 20−400 μM. No changes in recovered transition curves were observed, demonstrating that no significant protein aggregation is present.

Protein solutions with the desired GdnHCl concentration were prepared by a "mixing" method described previously (*22*). This procedure allows one to minimize variability with respect to protein concentration as well as reaching the equilibrium. Specifically, a solution containing folded protein was added to one containing unfolded protein (in 6 M GdnHCl) at identical protein concentration and in reverse order. Each sample was equilibrated for at least 1 h prior to measurements. This time is sufficient for completion of the (un)folding reaction induced by GdHCl, which is known to occur on the millisecond time scale (*14*, *15*). No changes in experimental data were observed after further 24 h.

Equilibrium (un)folding as a function of GdnHCl concentration was monitored by circular dichroism, steady-state, and time-resolved fluorescence. The apparent fraction of folded molecules was extracted from each set of raw data, assuming the two-state model (*13*):

$$f_N = \frac{X - X_U}{X_N - X_U} \quad (1)$$

In eq 1 the experimental parameter measured at a given GdnHCl concentration (e.g., fluorescence quantum yield, lifetime, ellipticity, etc.) is denoted as X, while X_N and X_U are the values of X characteristic of the folded and unfolded conformations, respectively, at the same denaturant concentration. The pre- and post-transition baselines were essentially flat as monitored by fluorescence and CD measurements. Hence, the X_N and X_U parameters were assumed to be independent of GdnHCl concentration. For fluorescence experiments, this assumption holds since the emission of the indole fluorophore in solution shows no significant change with GdnHCl concentration (*22*). In addition, we have no evidence that in the unfolded state (under native or native-like conditions) the Trp residue is exposed to the solvent, justifying such baseline correction for the present case.

Circular Dichroism Measurements. Circular dichroism measurements were carried out on a J-720 spectropolarimeter (JASCO, Japan) equipped with a temperature control system (NESLAB, USA). The spectropolarimeter was calibrated with (+)-10-camphorsulfonic acid. Far-UV spectra were recorded over 200−260 nm for a 50 μM protein sample in a 0.1 cm cell. Near-UV spectra were obtained over 250−350 nm for 50 and 400 μM protein samples in 1 and 0.2 cm cells, respectively. Each spectrum (the average of 10 scans) was corrected for the appropriate solvent-blank, and, thereafter, smoothed with J-720 software. Raw data were expressed as molar ellipticity in units of $deg\cdot cm^2\cdot dmol^{-1}$ (*23*). Measurements were performed with a bandwidth of 1 nm, a response time of 0.5 s, and a scan speed of 20 nm/min.

Steady-State Fluorescence Measurements. Fluorescence spectra were obtained for 20 μM protein samples on a SPEX Fluorolog-2 spectrofluorometer using the DM-3000 software (data interval of 0.5 nm, scan speed of 50 nm/min). Emission

was measured under "magic angle" conditions in the ratio mode and corrected for the appropriate solvent-blanks, as well as for wavelength-dependent bias of the optics and detection system. An excitation wavelength of 295 nm was used in most of the experiments to avoid tyrosine absorbance. For selected experiments (see below), the excitation was set at 280 nm. The emission was characterized by the quantum yield, ϕ, the position of the intensity maximum, λ_{max}, and the width of the spectral distribution, $\Delta\lambda_{1/2}$. The quantum yield, ϕ_{prot}, was determined by comparison with an aqueous solution of twice-recrystallized *N*-acetyltryptophanamide (standard) with $\phi_{st} = 0.14$ (*24*):

$$\phi_{prot} = \phi_{st}\frac{F_{prot}\,D_{st}}{F_{st}\,D_{prot}} \tag{2}$$

where D is the absorption and F is the fluorescence intensity integrated over the range of 300−450 nm. For native protein, ϕ_N was measured to be 0.26, while in the unfolded state (6 M GdnHCl) a value of 0.08 was obtained. The position of the emission maximum, λ_{max}, was recovered from the first-derivative plot of the emission spectrum, as the wavelength corresponding to the zero value of the first derivative. We also calculated the intensity-weighted average emission wavelength, $\langle\lambda_{max}\rangle$, as follows:

$$\langle\lambda_{max}\rangle = \frac{\sum_i \lambda_i F(\lambda_i)}{\sum_i F(\lambda_i)} \tag{3}$$

where $F(\lambda_i)$ is the fluorescence intensity measured at the emission wavelength λ_i.

Time-Resolved Fluorescence Measurements. Time-resolved fluorescence measurements were carried out by the time-correlated single-photon counting technique as described previously (*25*). Samples were excited at 295 nm using a synchronously pumped, frequency doubled, cavity-dumped dye laser (repetition rate of 4 MHz, pulse width of 5 ps, average UV power <200 μW). The channel width was 42 ps, and the data were collected in 1014 channels. The monochromator and microchannel plate photomultiplier combination yielded a transit time spread of 120 ps, allowing one to resolve correlation times as short as 50 ps.

Fluorescence intensity decays were collected under "magic angle" conditions for equal dwell times and by stepping the emission monochromator in increments of 5 nm in the range of 300−450 nm. Over 30 decays were obtained for each sample and simultaneously analyzed according to the global procedure (*26*), assuming that fluorescence intensity decay follows a multiexponential law:

$$I(t, \lambda) = \sum_i^n \alpha_i(\lambda) e^{-t/\tau_i} \tag{4}$$

The relative amplitudes, α_i, and the decay constants, τ_i, were the numerical parameters recovered. To resolve the emission spectra associated with the individual decay constant (decay-associated spectra, DAS), the fluorescence intensities at the various wavelengths were expressed as $\alpha\tau$ products, and the relative contribution of each decay component to the total emission was calculated as $\alpha_i\tau_i/\Sigma\alpha_i\tau_i$ (*27*). In all cases, two decay times and a third, short-lived, fixed component (compensating for any scattered excitation or color shift) gave the best fit.

To generate the anisotropy decay, $r(t)$, the fluorescence at 350 nm was monitored through a film polarizer oriented parallel, $I_{VV}(t)$, or perpendicular, $I_{VH}(t)$, to the vertical excitation polarization and alternatively recorded. Data were collected up to 20 000 counts in the peak. For each sample, eight pairs of intensity decays were measured sequentially and summed to calculate the anisotropy decay, $r(t)$, as follows:

$$r(t) = \frac{I_{VV}(t) - GI_{VH}(t)}{I_{VV}(t) + 2GI_{VH}(t)} = \frac{D(t)}{S(t)} \tag{5}$$

The factor G was reduced to unity with a wedge depolarizer (Optics for Research, DPU) placed 1 cm from the entrance slit of the monochromator. The parameters of the anisotropy decay were recovered from the experimental decays $I_{VV}(t)$ and $I_{VH}(t)$ by the "sum and difference" method assuming the nonassociative model (*28*). The anisotropy decay $r(t)$ was considered to be a sum of discrete exponential functions:

$$r(t) = \sum_i^n \beta_i e^{-t/\phi_i} \tag{6}$$

where β_i and ϕ_i were the numerical parameters recovered to ensure the best fit of the $D(t)$ function.

In all time-resolved fluorescence experiments, the reference lamp profile and color shift used for convolution analysis were tested with a monoexponential standard (melatonin aqueous solution with fluorescence lifetime $\tau_{fl} = 5.2$ ns). The convolution was compared with the experimental decay by a nonlinear least-squares analysis. The best fit between the theoretical curve and the data was evaluated from the plot of weighted residuals, the autocorrelation function of the weighted residuals, and the reduced χ^2 value. Estimation of error in the fitting parameters was done using the "χ^2_R-surface" plane method (*29*, *30*). The uncertainty in the recovered variable was calculated on the basis of a 90% confidence interval (*29*), which usually corresponds to a 10% increase in the χ^2_R minimum value (*31*).

Regarding the tryptophan dynamics, the decrease of anisotropy was considered to be caused by independent motions of the tryptophan reporter with corresponding correlation times ϕ_i (see eq 6). The most feasible model employed to analyze nanosecond dynamics of tryptophan in polypeptide chains considers the fast motions as oscillations (torsional vibrations) of an indole ring within the allowed conformer well (*25*, *32*). The slow motions include the rotations of the tryptophan residue together with the entire protein, with a backbone segment, as well as the rotation of the indole ring about $C_\alpha-C_\beta$ and $C_\beta-C_\gamma$ bonds (*25*, *32*). Since a broad spectrum of motions is possible in long-chain molecules, anisotropy experiments report the average diffusion coefficient, or harmonic mean time of motions that are comparable in time scale (*16*, *33*). In this regard, it should be pointed out that a large body of dynamic data for synthetic macromolecules in solutions reveal that this average parameter of the relaxation spectrum is a sensitive indicator of

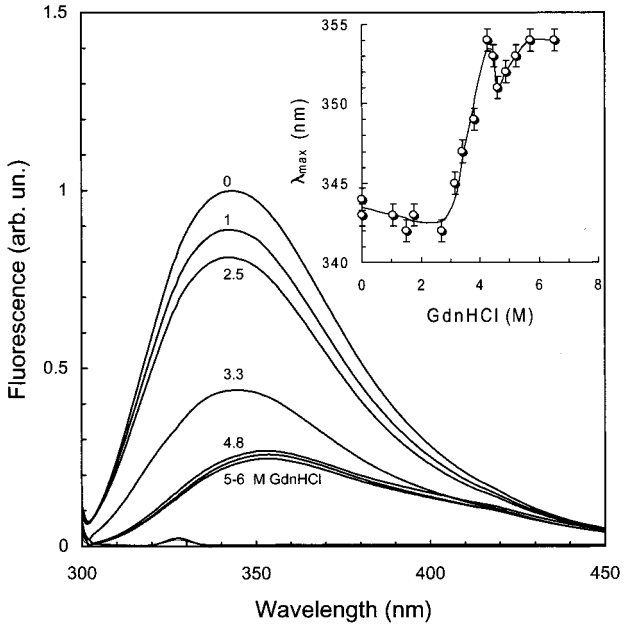

FIGURE 2: Fluorescence spectra of 16 μM GB1 in 20 mM sodium phosphate buffer (pH 5.7, 20 °C) for varying GdnHCl concentration. A buffer spectrum is given at the bottom for reference. The inset shows the variation of the emission maximum with increasing GdnHCl concentration. The excitation wavelength was 295 nm.

structure formation. Specifically, substantial changes were observed upon formation of local internal structures, or for the coil−helix and coil−globule transitions (*16*). A variety of intermediate structures exhibiting different intra-macromolecular dynamics were found in folding studies of Trp-containing synthetic polypeptides (*32*). Thus, analysis of fluorescence anisotropy data allows to extract information about structure formation during folding, which is difficult to recover by other experimental means. In the subsequent discussion, a relaxation time, $\tau = 3\phi$, will be used to compare the present data to prior results obtained by conventional steady-state methods (*16, 34*). In addition, the change in dynamics caused by a change in the solvent viscosity was taken into account (*16, 25*), and the relaxation times obtained experimentally were adjusted to the viscosity of water at 20 °C ($\eta = 1.005$ cP).

Viscosity Measurements. Specific viscosity was obtained with an Ostwald capillary viscometer having a water flow time of 140 s. For each sample, the results were averaged for three independently prepared solutions, each measured 10 times. The measurements were done at five protein concentrations varying from 0.5 to 2.5 mM. The solution and solvent densities were estimated by using 10 mL pycnometers calibrated with distilled water, and by refractive index measurements. The intrinsic viscosity was based on reduced specific viscosity plotted versus protein concentration (in g/100 mL) and extrapolated to zero concentration (*35*).

RESULTS AND DISCUSSION

Steady-State Fluorescence and Circular Dichroism. Unfolding of GB1 induced by GdnHCl (pH 5.7, 20 °C) resulted in a red shift of the emission spectrum and about a 3-fold drop in the fluorescence quantum yield (Figure 2). Far-UV CD spectra recorded for increasing GdnHCl concentrations decreased in amplitude, due to the loss of secondary structure in the unfolding transition (Figure 3a). In contrast, near-UV CD spectra altered significantly in both shape and amplitude, i.e., changed in a nonlinear fashion over the entire wavelength region (Figure 3b). Both fluorescence and CD data correspond well to those reported previously for GB1 and its close analogues (*14, 36*−*40*).

We monitored the unfolding transition by measuring the far-UV molar ellipticity at 222 nm, the near-UV ellipticity at 275 nm, and the fluorescence quantum yield. The fraction of folded molecules was calculated using eq 1, assuming the two-state model. Figure 4 demonstrates that the CD profiles superimpose perfectly on those derived from fluorescence. A sharp transition is observed in the 2−4 M GdnHCl range. The thermodynamic parameters recovered from the unfolding curves, i.e., $\Delta G_{water} = -5 \pm 0.4$ kcal·mol^{-1} and $m_g = -1.8 \pm 0.1$ kcal·(mol·M)$^{-1}$, are identical to those in previous reports (*14, 38*). In fact, steady-state fluorescence and CD data show that formation of the native-like W43 environment (fluorescence), tight packing of the aromatic groups (near-UV CD), and formation of native secondary structure (far-UV CD) apparently occur under identical conditions, seemingly supporting the two-state transition assumption. Unexpected changes in the near-UV CD data, however, prompted us to examine this further. Figure 3b shows that the different parameters of the near-UV CD spectrum, e.g., θ_{275} and θ_{293}, track the unfolding in a different way, exhibiting large or small changes. In fact, in the region from 270 to 300 nm the main contribution to the CD spectrum arises from tryptophan and tyrosine residues, while the band near 290 nm is attributed to the ^1L_b transition of tryptophan alone (*23*). Note that the tryptophan band near 290 nm appears at 4 M GdnHCl and its amplitude shows no significant change during folding. This finding might indicate that defined structural changes occur under extensively denaturing conditions and the W43 aromatic side chain is thus transferred to an asymmetric environment.

Indication of changes in the W43 microenvironment above 4 M GdnHCl can also be derived from the analysis of the emission maximum, λ_{max}. In contrast to the continuous decrease in fluorescence intensity, λ_{max} followed the unfolding in a nonmonotonic way (Figure 2, inset). It shifted over the range of 2−4 M GdnHCl from the native value of 343 ± 1 nm to 354 ± 1 nm. Further increase in GdnHCl concentration to 4.6 M led to an abrupt shift to 351 ± 1 nm, followed by a reverse shift to 354 nm at 6 M GdnHCl. The blue-shifted emission in the native state is consistent with the partially buried W43 in the hydrophobic core of the protein, as observed in NMR and X-ray structures (*17, 41*−*43*). The position of the emission maximum in the unfolded state reflects the high polarity of the W43 microenvironment in 6 M GdnHCl. A similar position of emission maximum has been observed on numerous occasions for low molecular weight tryptophan derivatives surrounded by charged carboxy or amino groups (*44*). It appears that the λ_{max} behavior in 4−6 M GdnHCl monitors changes in the dielectric constant of the W43 microenvironment. Note that a more sophisticated analysis in terms of the intensity-weighted average emission wavelength (center of gravity) corroborates the λ_{max} data.

Steady-state fluorescence experiments with varying excitation wavelength provide supplementary evidence for local conformational rearrangements of the region around W43 under highly denaturing conditions. We find that by using excitation at 280 nm an additional emission appears in the

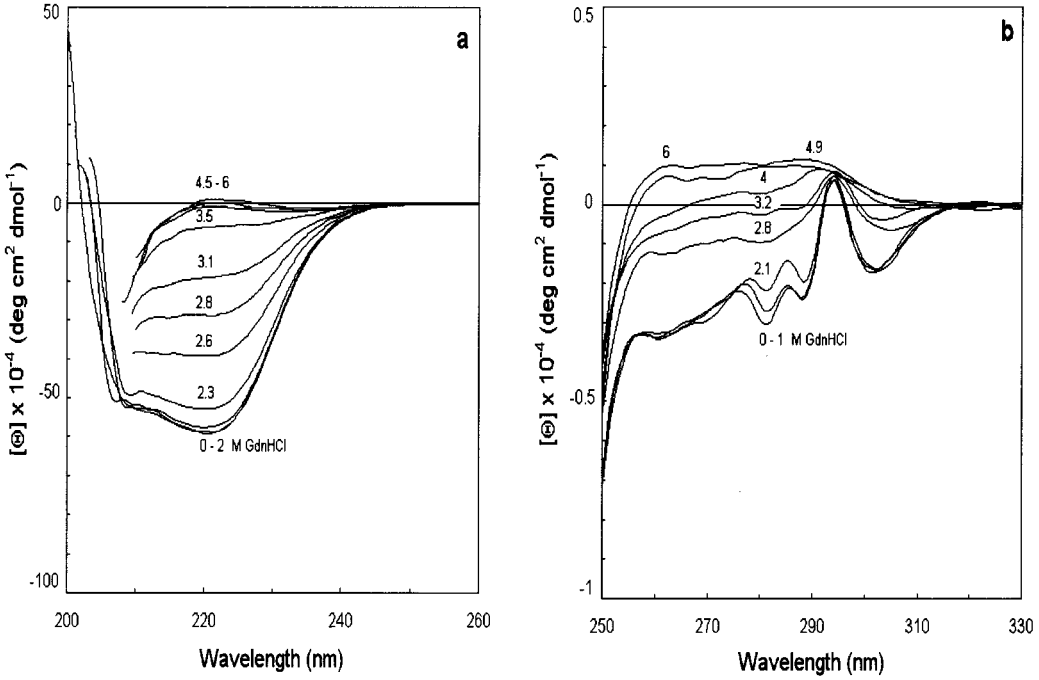

FIGURE 3: Far-UV (a) and near-UV (b) circular dichroism spectra of GB1 in 20 mM sodium phosphate buffer (pH 5.7, 20 °C) for varying GdnHCl concentration. The conditions were as described under Materials and Methods.

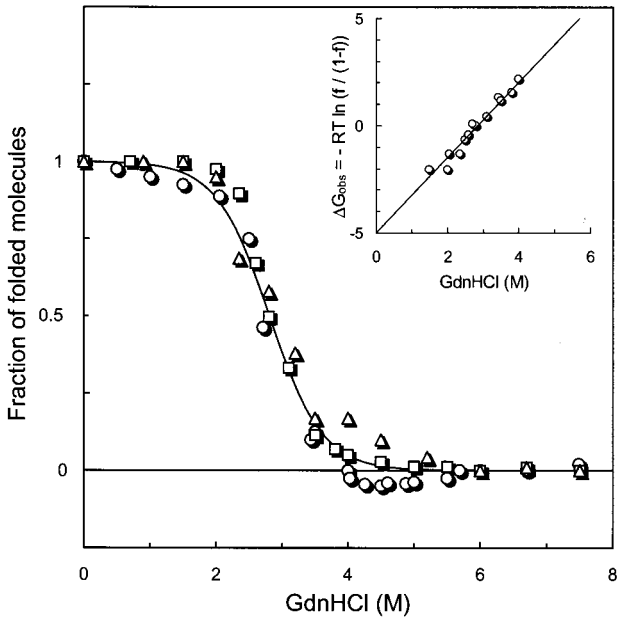

FIGURE 4: Equilibrium GdnHCl denaturation curves for GB1 in 20 mM sodium phosphate buffer (pH 5.7, 20 °C). The (un)folding transition was followed by the ellipticity at 222 nm (□), the ellipticity at 275 nm (△), and the intrinsic fluorescence excited at 295 nm (○). Raw data were converted by eq 1 to the fraction of folded molecules, *f*, and plotted against GdnHCl concentration. The solid line is the nonlinear least-squares fit of the data to the equation: $f/(1 - f) = \exp[-(\Delta G/RT)]$. The inset shows the free energy of folding as a function of GdnHCl concentration.

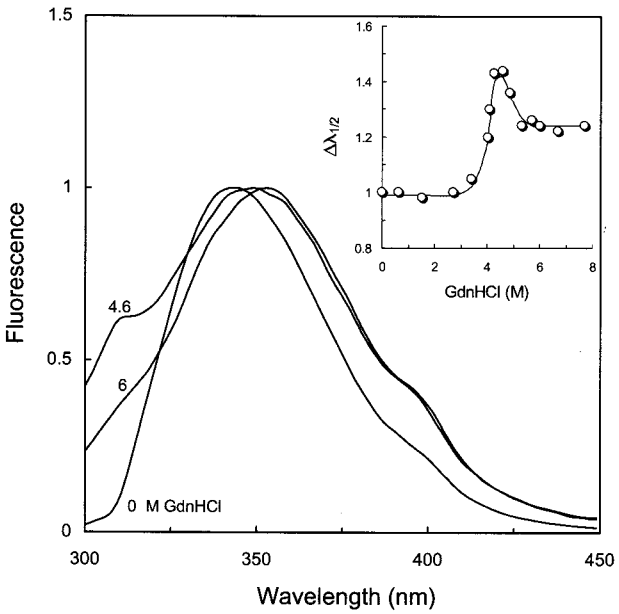

FIGURE 5: Effect of GdnHCl on the emission at 310 nm in the fluorescence spectrum of GB1. Fluorescence was excited at 280 nm, and the spectra were normalized to the intensity at the maximum. The inset shows the effect of [GdnHCl] on the width of spectral distribution ($\Delta\lambda_{1/2}^{native} = 55$ nm). Other experimental conditions were as described for Figure 2.

GB1 fluorescence spectrum. Changes in protein fluorescence with variation of GdnHCl concentrations are shown in Figure 5. The emission at 310 nm is clearly visible at 4.6 M GdnHCl and disappears once the protein is folded. Evidently, excitation at 280 nm activates both tryptophan and tyrosine residues. To assign this band to particular aromatic residues, we constructed a GB1 mutant containing only a single tyrosine residue, namely, Y45, replacing the two others, Y3 and Y33, by phenylalanines. Using the single tyrosine mutant protein, the emission spectrum was identical to that of the wild-type protein; therefore, we assign the shoulder at 310 nm to the aromatic residues W43 and Y45 residing on the β-strand 3. To monitor the spectral changes induced by the appearance of the emission at 310 nm, we calculated the width of the spectral distribution, $\Delta\lambda_{1/2}$, normalized to that in the native state and plot it as a function of GdnHCl concentration. Figure 5 shows that this parameter does not track the unfolding transition in a two-state manner, exhibiting a maximum at 4.6 M GdnHCl.

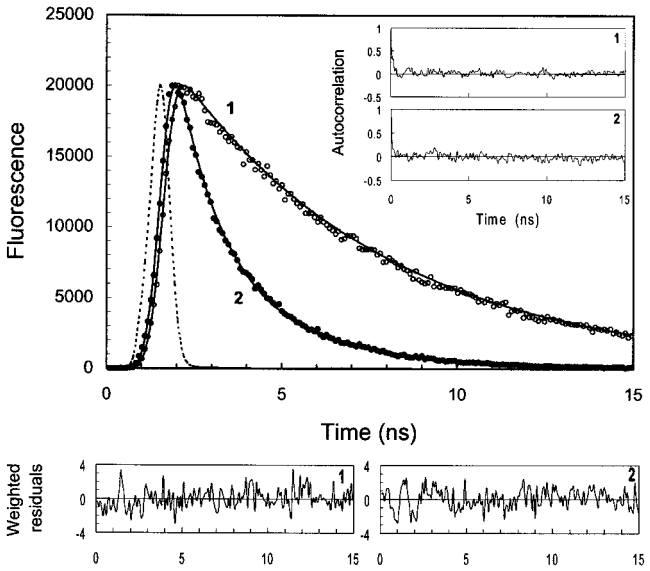

FIGURE 6: Time-resolved fluorescence intensity decay of GB1 in the native state (1) and unfolded state in 6 M GdnHCl (2). The experimental data (circles), fitted curves (solid curve), and scaled lamp profile (dotted curve) are shown. Weighted residuals are displayed at the bottom. The inset shows the autocorrelation function of the weighted residuals. The excitation was set at 295 nm, and emission was collected at 350 nm. The protein concentration was 10 μM in 20 mM sodium phosphate buffer at pH 5.7 and 20 °C.

Time-Resolved Fluorescence Intensity. Fluorescence intensity kinetics of the single tryptophan residue were adequately described by a biexponential model over the entire range of GndHCl concentrations:

$$I(t) = \alpha_{short} e^{-t/\tau_{short}} + \alpha_{long} e^{-t/\tau_{long}} \qquad \sum \alpha_i = 1 \quad (7)$$

The reduced χ^2_R value, characterizing the goodness of the fit, was always less than 1.5, and the weighted residuals and the autocorrelation of the residuals were randomly distributed around zero. Attempted fits of the experimental data to one- or two-exponential models with the fixed mean decay constants recovered for native and unfolded molecules showed a substantial (>20%) increase in the χ^2_R value. Since a three-exponential fit led to no improvement in χ^2_R, the simpler two-exponential model was chosen for further consideration. A typical example of the analysis of the experimental data is shown in Figure 6. Parameters associated with the fluorescence intensity decays obtained at different GdnHCl concentrations are summarized in Table 1 together with χ^2_R values used to judge the quality of the fit.

Fluorescence kinetics employed to monitor the unfolding reaction, obviously, might reflect both the complex relaxation of the tryptophan excited state in a particular conformation state as well as that in the mixture of global conformations (i.e., native and unfolded). In fact, Table 1 shows that for unfolded protein, in the range of 4.9−6 M GdnHCl, the W43 fluorescence exhibits no changes with GdnHCl concentration as expected for the indole fluorophore in solution (*22*). The spectra associated with the individual decay components (DAS) are indistinguishable by the position of emission maximum and spectral distribution (Figure 7a). Since the positions of emission maxima for folded and unfolded proteins are shifted by about 10 nm (inset, Figure 7), decay components recovered for GB1 under extensively denatured conditions cannot be assigned to fully unfolded and folded conformations. Indeed, the invariant DAS positions hint at the quasi-homogeneous environment of the apparent fluorescence species. Therefore, it seems most likely that the fluorescence kinetics recorded in the 4.9−6 M GdnHCl range report on the complex electronic relaxation of the W43 residue in the unfolded chain. This complexity might originate from a multitude of tryptophan isomers or rotational isomers of nearby quenching residues.

Table 1: Parameters Associated with Tryptophan Fluorescence Intensity Decay in GB1

	fluorescence lifetime				
GdnHCl (M)	τ_{short}, ns	τ_{long}, ns	α_{short}[a]	$\langle\tau\rangle$,[b] ns	χ^2_R
0	0.44	5.9	0.18	4.9	1.18
0.6	0.48	5.7	0.15	4.9	1.1
	0.46 ± 0.02	5.8 ± 0.1	0.16 ± 0.02	4.9	
1.5	2.1	5.4	0.19	4.8	1.28
2.7	1.8	5.1	0.37	3.9	1.4
3.4	1.5	4.5	0.65	2.6	1.04
3.6	1.5	4.4	0.72	2.3	1.05
4	1.6	4.4	0.77	2.2	1.28
	1.7 ± 0.2	4.8 ± 0.4			
4.1	1.4	3.7	0.77	1.8	0.99
4.3	1.3	3.2	0.73	1.8	1.36
4.5	1.2	3.1	0.71	1.8	1.27
4.6	1.2	3.0	0.7	1.8	1.16
	1.3 ± 0.1	3.3 ± 0.3		1.8	
4.9	1.1	2.9	0.6	1.8	1.01
5.3	1	2.7	0.61	1.6	1.11
5.7	1	2.5	0.58	1.7	1.32
6	1.1	2.6	0.6	1.7	1.19
	1.05 ± 0.05	2.7 ± 0.2	0.60 ± 0.01	1.7 ± 0.1	

[a] Fraction of short-lived component as measured at 350 nm. [b] Mean decay time $\langle\tau\rangle = \Sigma\alpha_i\tau_i$.

Decreasing the GdnHCl concentration further, to 4 M, results in changes of the W43 fluorescence, and the fraction of the short-lived component, α_{short}, increases by almost 30%. Figure 8 summarizes the fluorescence decay data and demonstrates that α_{short} depends on GdnHCl concentration in a nonmonotonic fashion, showing a maximum value at ~4 M GdnHCl. This indicates that changes in interactions involving W43 occur at relatively high denaturant concentration, namely, in the interval between 4 and 4.9 M GdnHCl.

Further, the lifetimes of short- and long-lived components recovered for the 1.5−4 M GdnHCl range correspond within 10% to the mean decay times measured for native (4.9 ns) and unfolded (1.7 ns) molecules (Table 1). Moreover, the changes in α_{short} agree well with the unfolding transition as monitored by mean decay time (Figure 8), steady-state fluorescence, and CD measurements (Figure 4).

The native protein exhibits nearly monoexponential fluorescence intensity kinetics, and the apparent population of the short-lived species is only about 15%. The lifetime of the short-lived component, however, has a value of 0.4 ns in the native state and 2 ns in 1.5 M GdnHCl. No significant changes in the long lifetime were observed in this range, where τ_{long} was measured as 5.8 ns. To illustrate these changes, we calculate the ratio of lifetimes, τ_{short}/τ_{long}, recovered from the fluorescence decay of W43. For the simplest two-state model, this parameter is expected to remain constant over the entire range of the denaturant concentrations. Figure 8 demonstrates that the lifetime ratio

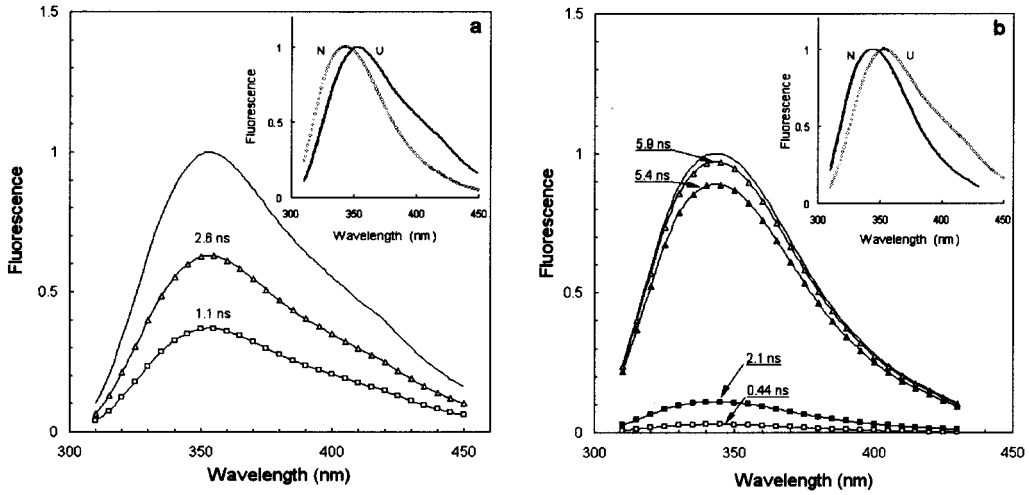

FIGURE 7: Resolution of the emission spectrum of GB1 in the unfolded state in 6 M GdnHCl (a) and the native state (b) into decay-associated spectra (DAS). The total emission spectrum (solid line without symbols) and each decay spectrum with long (△) and short (□) lifetimes are shown. For the native state (b), spectra of GB1 at 1.5 M GdnHCl are also displayed (filled symbols). The inset shows normalized DAS recovered for unfolded and native states. The experimental conditions were as described for Figure 6.

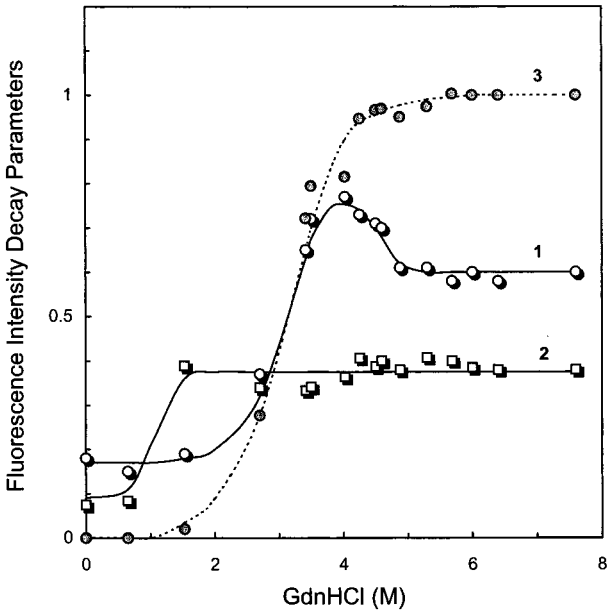

FIGURE 8: Parameters associated with the tryptophan fluorescence intensity decay. The fraction of the short lifetime component, α_{short} (1), and the fluorescence lifetime ratio, τ_{short}/τ_{long} (2), are shown for various GdnHCl concentrations. The apparent fraction of unfolded molecules as monitored by the mean decay time, $\langle\tau_{fl}\rangle$ (3), is given for reference. The experimental conditions were as described for Figure 6.

changes cooperatively from 0.08 to 0.4 over the 0−1.5 M GdnHCl range with no further significant changes up to 6 M GdnHCl. A shallow minimum, however, is present, which we refrain to analyze given the experimental accuracy. Most important, the decay-associated spectra generated for GB1 at 0−1.5 M GdnHCl (pre-transition range) are indistinguishable by the position of the emission maximum at ∼342 nm, suggesting the quasi-homogeneous nativelike environment of the apparent fluorescence species (Figure 7b). In fact, the double exponential kinetics recorded over the pre-transition range report both the complex fluorescence of W43 buried in the protein core and the changes in W43 fluorescence during formation of the native structure. The dynamic quenching of the short-lived component in native molecules may be caused by the proximity of a quencher, i.e., by another amino acid close in space to W43. Inspection of the GB1 structure reveals that in the native state residue K31, residing on the α-helix, is in close contact (27 atoms within the sphere of 5 Å) with W43. Since lysine residues are capable of being strong quenchers of indole fluorescence (*45*), we suggest that in ∼1 M GdnHCl we observe the melting of the interface between the α-helix and the *β*-sheet, e.g., an increase in the mutual distance or change in mutual orientation of W43 and K31. Regarding GB1 folding, this observation suggests that disruption of tertiary structure might be a stepwise process beginning with loosening of the structure at the weakest point in the native fold (*46*). Further studies on the interaction of hydrophobic dyes with the protein molecules, fluorescence energy transfer, and also lifetime distribution analysis of the W43 fluorescence might be useful to clarify specific features of these intermediate structures.

Time-Resolved Fluorescence Anisotropy. Nanosecond dynamics of W43 were measured for a series of GdnHCl concentrations. Two correlation times are needed to account for the fluorescence anisotropy decay data, and the attempted fits to a one-exponential model showed a 2-fold increase in the χ^2_R value. Addition of a third exponential led to no improvement to χ^2_R. The parameters associated with the decay of W43 fluorescence anisotropy are summarized in Table 2. Figure 9 illustrates the changes in anisotropy kinetics caused by the unfolding of the protein from the native state to the denatured state in 6 M GdnHCl.

The apparent "zero-time" anisotropy, r_0, follows the (un)-folding in a two-step manner exhibiting a change from 0.22 ± 0.02 to 0.16 ± 0.02 in the 2−4 M GdnHCl range (Figure 10a). These values were observed on numerous occasions in studies of tryptophanyl derivatives *(44)*, as well as a wide range of polypeptides and proteins (*25*). The former value is expected for a tryptophan residue in a rigid environment, while the latter one is indicative of very fast librations of the indole ring within the unfolded polypeptide chain. The fast motion of W43 shows no change upon (un)folding and has an average relaxation time of 0.8 ± 0.3 ns over the entire range of GdnHCl concentrations (Figure 10b). The amplitude

Table 2: Parameters Associated with Tryptophan Fluorescence Anisotropy Decay in GB1[a]

	correlation times[b] (ns)		amplitudes		
GdnHCl (M)	ϕ_{fast}	ϕ_{slow}	β_{fast}	β_{slow}	χ_R^2
0	0.41	3.1	0.01	0.19	1.19
0.6	–	3.1	–	0.22	1.18
1.5	0.21	3.4	0.01	0.21	1.34
2.3	0.4	4	0.04	0.17	1.42
2.7	0.16	4.2	0.09	0.17	1.14
3	0.3	4.2	0.07	0.13	1.02
3.4	0.5	5.5	0.06	0.1	1.04
3.6	0.53	7.6	0.06	0.1	1.13
3.8	0.38	4.8	0.06	0.08	1.39
4	0.3	2.9	0.10	0.08	1.24
4.1	0.32	3	0.08	0.09	1.49
4.3	0.27	2.5	0.08	0.09	1.22
4.5	0.55	2.5	0.08	0.08	1.38
4.6	0.51	2.4	0.08	0.08	1.05
4.9	0.42	2.3	0.07	0.08	1.11
5.3	0.35	2.1	0.09	0.08	1.16
5.7	0.25	2.4	0.08	0.08	1.01
6	0.42	2.4	0.08	0.075	1.28

[a] The error in the values of recovered parameters is about 10% as has been estimated through the analysis of χ^2 surfaces (see Materials and Methods) and results of replication. [b] In further analysis, the change in dynamics caused by solvent viscosity was taken into account, and the relaxation times, $\tau = 3\phi$, experimentally obtained were adjusted to the viscosity of water at 20 °C ($\eta = 1.005$ cP).

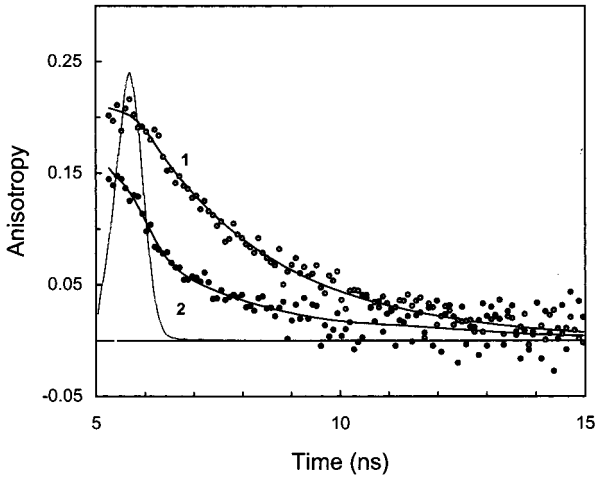

FIGURE 9: Time-resolved fluorescence anisotropy decay of GB1 in the native state (1) and in the unfolded state at 6 M GdnHCl (2). The experimental data (circles), fitted curves (solid line), and scaled lamp profile (gray line) are shown. The excitation was set at 295 nm, and emission was collected at 350 nm. The protein concentration was 10 μM in 20 mM sodium phosphate buffer at pH 5.7 and 20 °C.

of fast motion, characterized by the parameter β_{fast} (see eq 6), was found to be a sensitive measure for the formation of native structure. Figure 11 shows that folding leads to a restriction of the fast motion, which most likely originates in torsional vibrations of the indole ring. The decrease in amplitude of torsional vibrations is evidently caused by increased steric repulsion and/or specific interactions of W43 with nearby amino acids. Importantly, (un)folding appears to occur in a three-step manner when monitored by β_{fast}: a sharp increase in β_{fast} occurs between 2 and 3 M GdnHCl, followed by a second, smaller increase around 4 M GdnHCl.

The most sensitive parameter monitoring the protein folding is the slow relaxation time, τ_{slow}, recovered from W43 fluorescence anisotropy decay. The relaxation time of ~9 ns measured on native GB1 agrees well with theoretical predictions for the overall rotation of the protein molecule, which can be derived from independent measurements, namely, the viscosity of the protein solution (*47*):

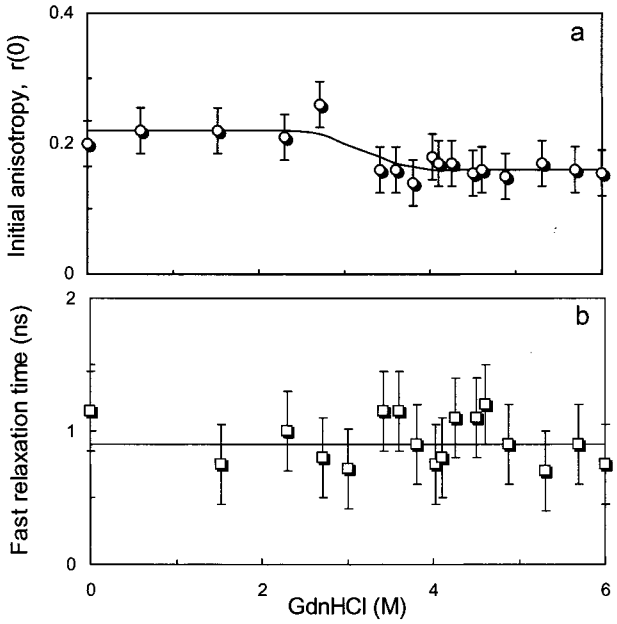

FIGURE 10: Parameters associated with the fluorescence anisotropy decay. The initial anisotropy (a) and the relaxation time of fast motion (b) are shown for various GdnHCl concentrations. The experimental conditions were as described for Figure 9.

$$\tau_{wh} = \frac{3[\eta]\eta M}{\nu(p)RT} = 3\phi \qquad (8)$$

Here M is the molecular weight of the protein, $[\eta]$ is the intrinsic viscosity of the protein solution, R is the gas constant, and T is the absolute temperature. The Simha factor, $\nu(p)$, is the numerical coefficient depending on the molecular shape, which for a nearly spherical particle has a value of 2.5 (*35*). Consequently, for native GB1 (6257 D) in aqueous solution ($\eta_{H_2O} = 1.005$ cP) at 20 °C with the experimental value of $[\eta] = 2.9 \pm 0.5$ cm^3/g, the relaxation time for overall rotation is expected to be about 9 ns. The agreement of the experimental and theoretical estimates suggests that any intramolecular nanosecond motions in the native GB1 are sufficiently hindered not to be seen in fluorescence anisotropy kinetics. The relaxation time due to the overall rotation of the unfolded GB1 chain in 6 M GdnHCl is expected to be about 120 ns. This estimate is based on the experimental value of the intrinsic viscosity of GB1 solution (6 M GdnHCl, 20 °C) of 25 cm^3/g (*25*). On the time scale of tryptophan fluorescence (~2 ns), this slow rotation has no measurable effect on anisotropy kinetics. Thus, the average relaxation time of 4 ns observed in the unfolded chain is basically identical to the average time of W43 intramolecular motions. Recently, we demonstrated that a motion with the time of 4−6 ns is typical for unfolded proteins, adrenocorticotropic hormones, and synthetic polypeptides (*25*). Most likely, the underlying process is the isomeric rotation of the indole ring about $C_\beta - C_\gamma$ bonds, i.e., the jump from one conformer well to another (*25*). Importantly, in the course of GB1 (un)folding, the anisotropy experiments recover time constants for different motions; i.e., the global protein

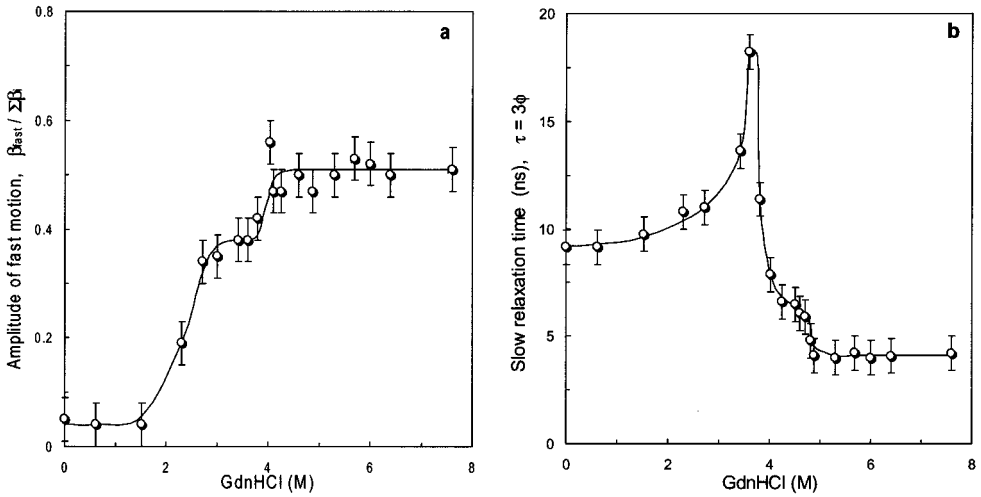

FIGURE 11: Amplitude of fast motion (a) and the slow relaxation process (b) observed in tryptophan fluorescence anisotropy kinetics upon GB1 unfolding induced by GdnHCl. The relaxation times obtained experimentally were adjusted to the viscosity of water at 20 °C (η = 1.005 cP). The experimental conditions were as described for Figure 9.

rotation is measured for the native state, and rotation of the W43 side chain is measured for the unfolded state in 6 M GdnHCl.

Figure 11 displays the values observed for the slow relaxation time as a function of GdnHCl concentration. Three distinguishable phases are clearly visible. Initially, the time increases from 9 ns in the native state to 18 ns in 3.8 M GdnHCl. This increase in relaxation time, which originally was attributed to overall rotation, may be due to the appearance of molecules with larger molecular dimensions. Next, a sharp decrease in time to 7 ns is observed between 3.8 and 4.2 M GdnHCl. This increase in the internal mobility of W43 (decrease in relaxation time) reflects the cooperative loss of intramolecular interactions involving the fragment of the polypeptide chain on which W43 resides. In the third stage, a further increase in W43 rotational freedom is observed, since the relaxation time drops to 4 ns in 6 M GdnHCl. At this stage, the internal mobility of W43 exhibits a value typical for the mobility of tryptophan in an unfolded polypeptide chain (*25*). Importantly, these second and third stages observed by time-resolved fluorescence anisotropy are both in conditions where GB1 exhibits no secondary structure as measured by CD and shows invariant steady-state fluorescence properties (see Figure 4).

Obviously, upon folding, the overall rotation ($\tau_{overall}$) becomes faster due to the greater compactness of the molecule, while the internal mobility (τ_{intra}) can slow due to increasing numbers of intramolecular interactions. If we assume that under the conditions corresponding to the maximum τ_{exp}, these opposing processes contribute about equally to the anisotropy decay:

$$\frac{1}{\tau_{exp}} \approx \frac{1}{\tau_{overall}} + \frac{1}{\tau_{intra}} \approx \frac{2}{\tau_{overall}} \approx \frac{2}{\tau_{intra}} \qquad (9)$$

then for τ_{exp} = 18 ns observed in 4 M GdnHCl, the $\tau_{overall}$ is expected to be around 36 ns. Since the time of overall rotation is directly related to the molecular size *(35)*, in 4 M GdnHCl the GB1 molecular volume is expected to be 4 times larger than in the native state. To support this notion, we performed intrinsic viscosity, [η], measurements in 4 M GdnHCl and obtained a value of 11 ± 3 cm^3/g at

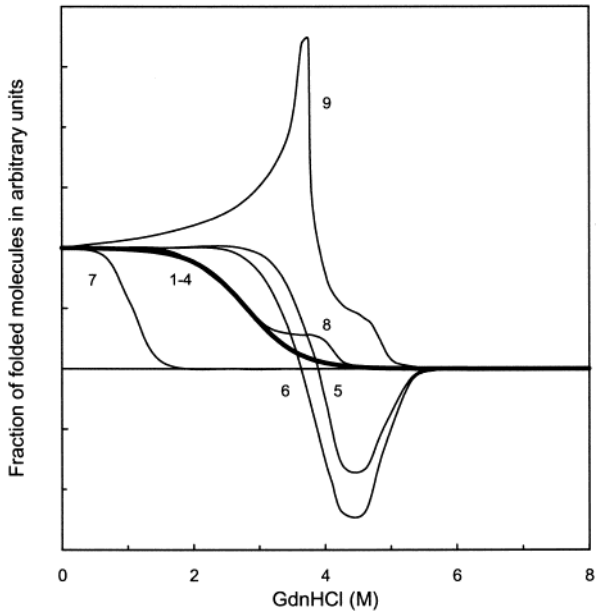

FIGURE 12: GdnHCl-induced unfolding of GB1 as monitored by ellipticity at 222 nm (1), ellipticity at 275 nm (2), intrinsic fluorescence (3), mean decay time (4), emission at 310 nm (5), fraction of the short-lived component in fluorescence intensity decay (6), ratio of time constants in fluorescence intensity decay (7), amplitude of the fast motion (8), and relaxation time of the slow motion (9).

20 °C. This finding indicates that the GB1 molecular volume in 4 M GdnHCl is significantly larger than that of native protein ([η] ~ 3 cm^3/g), yet substantially smaller than that of the unfolded GB1 chain in 6 M GdnHCl ([η] ~ 25 cm^3/g). Based on intrinsic viscosity and nanosecond dynamics measurements, we believe that the second step in GB1 folding is the formation of an initial collapsed state.

Figure 12 summarizes all parameters measured in the present study, vividly demonstrating that different intrinsic probes yield non-overlapping unfolding. Specifically, the CD, steady-state fluorescence, and mean decay time data support a two-state model of (un)folding and provide no evidence for the existence of any significantly populated intermediates over a wide range of GdnHCl concentration. This, however, does not completely reflect the conformational rearrangement

of the protein molecule. This conclusion is supported by the appearance of an emission at 310 nm, by the changes in the fluorescence intensity decay, and by the variation in emission maximum and tryptophan nanosecond mobility. The noncoincidence of all transitions monitored by different molecular probes suggests that equilibrium intermediates appear in GB1 unfolding. Most interestingly, these intermediates occur prior to the formation of α-helical structure in the protein.

The first distinct species in equilibrium folding is observed at ∼4.6 M GdnHCl. The decrease in tryptophan mobility and the changes in emission suggest the involvement of the W43 side chain in intramolecular interactions. Clearly, such perturbations of the tryptophan fluorescence may be due to relatively local events, not involving the complete domain or overall folding. No substantial changes in the molecular dimensions are observed within the range of 4.6−6 M GdnHCl, as judged by the intrinsic viscosity measurements. Therefore, we suggest that this first intermediate, U_1, most likely relates to the formation of the 41−56 hairpin fragment, a conclusion supported by results of fragment reconstitution experiments (*37, 48*−*50*). Studies of the conformational properties of fragments comprising the GB1 secondary structure have shown that in a β-hairpin containing residues 41−56 some folded structures persist even under highly denaturing conditions (*48, 50*). Recently, experimental evidence that this fragment may contain a folding nucleation site was obtained by NMR spectroscopy for urea-induced denaturation of GB1 (*51*). Together, these studies provide strong evidence that the 41−56 fragment is an important initiation site in the folding of the GB1 chain.

The second conformational intermediate, U_2, was suggested by the cooperative decrease in tryptophan mobility and by changes in intrinsic viscosity. Both parameters are related to molecular collapse, rendering the protein compact prior to formation of α-helix and progressive formation of the native tight packing. Therefore, the main difference between U_1 and U_2 is the degree of compactness. The GB1 molecular volume in the U_1 conformation differs very little from that in the unfolded state in 6 M GdnHCl at 20 °C, whereas in the U_2 conformation it decreases to about half of its original volume. The nature of the structural elements that might be present in the collapsed intermediates is unclear. Yet, the obvious lack of any rigid secondary structure points to a hydrophobic collapse of the protein chain. This is in agreement with results of earlier NMR studies on GB1 which have shown (*14*) that protection factors for ND−NH exchange in the initial collapsed state (in 4 M GdnHCl) are 10-fold higher than would be expected for a random coil. Interestingly, a similar initial hydrophobic collapsed state has been observed recently in the folding of barstar (*8*), which is another small single-domain α/β protein. It may well be the case that partially folded intermediates as revealed by the present study are a common feature of α/β protein folding. All the data together on GB1 suggest to us the following scenario: upon folding, the 41−56 segment first forms a stable (or semistable) β-hairpin structure by diffusion from chaotropic solution, which undergoes an interaction with the 1−40 segment (helix and second β-hairpin), followed by formation of the rigid native structure. More specific information about the structure of these partially folded intermediates can be obtained by fluorescence energy transfer experiments, which are in progress.

In summary, employing multi-parametrical experiments allows one to probe different aspects of intramacromolecular structure formation and yields valuable information above and beyond any single type of experiment. More important, this multi-parametrical approach may provide a sound basis for generating structural details of equilibrium folding intermediates with known features, expanding the conventional, two-state view of folding.

ACKNOWLEDGMENT

We are grateful to Oleg B. Ptitsyn, who initiated this work and was inspirational for all data analysis. We express our appreciation to Robert Jernigan and James Hofrichter for carefully reading the manuscript and valuable discussion and to William A. Eaton for generous use of equipment. We thank Joshua Sampson for preparation of the GB1 mutant and Tom Bradrick for help in anisotropy experiments.

REFERENCES

1. Privalov, P. L. (1992) in *Protein Folding* (Creighton, T. E., Ed.) pp 83−126, W. H. Freeman & Co., New York.
2. Karplus, M., and Shaknovich, E. (1992) in *Protein Folding* (Creighton, T. E., Ed.) pp 127−195, W. H. Freeman & Co., New York.
3. Uversky, V. N., and Ptitsyn, O. B. (1994) *Biochemistry 33*, 2782−2791.
4. Uversky, V. N., and Ptitsyn, O. B. (1996) *J. Mol. Biol. 255*, 215−228.
5. Kiefhaber, T., Labhardt, A. M., and Baldwin, R. L. (1995) *Nature 375*, 513−515.
6. Hoeltzli, S. D., and Frienden, C. (1995) *Proc. Natl. Acad. Sci. U.S.A. 92*, 9318−9322.
7. Swaminathan, R., Nath, U., Udgaonkar J. B., Periasamy, N., and Krishnamoorthy, G. (1996) *Biochemistry 35*, 9150−9157.
8. Nath, U., and Udgaonkar J. B. (1997) *Biochemistry 36*, 8602−8610.
9. Bhuyan A. K., and Udgaonkar J. B. (1998) *Biochemistry 37*, 9147−9155.
10. Garcia, P., Merola, F., Receveur, V., Blandin, P., Minard, P., and Desmadril, M. (1998) *Biochemistry 37*, 7444−74455.
11. Carlsson, U., and Johnsson, B.-H. (1995) *Curr. Opin. Struct. Biol. 5*, 482−487, and references cited therein.
12. Shortle, D. R. (1996) *Curr. Opin. Struct. Biol. 6*, 24−30.
13. Ptitsyn, O. B. (1995) *Adv. Protein Chem. 47*, 83−229.
14. Kuszewski, J., Clore, G. M., and Gronenborn, A. M. (1994) *Protein Sci. 3*, 1945−1952.
15. Park, S.-H., Shastry, M. C. R, and Roder., H. (1999) *Nat. Struct. Biol. 6* (10), 943−947.
16. Anufrieva, E. V., and Gotlib, Yu. Ya. (1981) *Adv. Polym. Sci. 40*, 1−68.
17. Gronenborn, A. M., Filpula, D. R., Essing, N. Z., Achari, A., Whitlow, M., Wingfield, P. T., and Clore, G. M. (1991) *Science 253*, 657−661.
18. Edelhoch, H. (1967) *Biochemistry 6*, 1948−1954.
19. Gill, S. C., and von Hippel, P. H. (1989) *Anal. Biochem. 182*, 319−326.
20. Nozaki, Y. (1972) *Methods Enzymol. 26*, 43−50.
21. Pace, C. N. (1986) *Methods Enzymol. 131*, 266−280.
22. Eftink, M. R. (1994) *Biophys. J. 66*, 482−503.
23. Woody R. W. (1996) in *Circular Dichroism and the Conformational Analysis of Biomolecules* (Fasman, G. D., Ed.) pp 25−69, Plenum Press, New York.
24. Eisinger, M. (1969) *J. Photochem. Photobiol. 9*, 247−258.
25. Tcherkasskaya, O., Ptitsyn, O. B., and Knutson, J. R. (2000) *Biochemistry 39*, 1879−1889.
26. Knutson, J. R., Beechem, J. M. and Brand, L. (1983) *Chem. Phys. Lett. 102*, 501−507.

27. Knutson, J. R., Walbridge, D. G., and Brand, L. (1982) *Biochemistry 21*, 4671−4679.
28. Beechem, J. M., Gratton, E., Ameloot, M., Knutson, J. R., and Brand, L. (1991) in *Topics in Fluorescence Spectroscopy* (Lakowicz, J. R., Ed.) Vol. 2, pp 241−305, Plenum Press, New York.
29. Johnson, M. L., and Faunt, L. M. (1992) *Methods Enzymol. 210*, 1−37.
30. Tcherkasskaya, O., Spiro, J. G., Ni, Sh., and Winnik, M. A. (1996) *J. Phys. Chem. 100*, 7114−7121.
31. Knutson, J. R. (1992) *Methods Enzymol. 210*, 357−374.
32. Semisotnov, G. V., Zikherman, K. Kh., Kasatkin, S. B., Ptitsyn, O. B., and Anufrieva E. V. (1981) *Biopolymers 20*, 2287−2309.
33. Lakowicz, J. R. (1999) *Principles of fluorescence spectroscopy*, 2nd ed., pp 347−368, Kluwer Academics/Plenum Publishers, New York.
34. Creighton, T. E. (1993) in *Proteins: Structure and Molecule Properties*, p 268, W. H. Freeman & Co., New York.
35. Cantor, C. R., and Schimmel, P. R. (1980) *Biophysical Chemistry*, Part 2, W. H. Freeman & Co., New York.
36. Alexander, P., Fahnestock, S., Lee., T., Orban, J., and Bryan, P. (1992) *Biochemistry 31*, 3597−3603.
37. Kobayashi, N., Honda, Sh., Yoshii, H., Uedaira, H., and Munekata, E. (1995) *FEBS Lett. 366*, 99−103.
38. O'Neil, K. T., Hoess, R. H., Raleigh, D. P., and DeGrado, W. F. (1995) *Proteins: Struct., Funct., Genet. 21*, 11−21.
39. Goward, C. R., Irons, L. I., Murthy, J. P., and Atkinson, T. (1991) *Biochem. J. 274*, 503−507.
40. Cregut, D., and Serrano, L. (1999) *Protein Sci. 8*, 271−282.
41. Achari, A., Hale, S. P., Howard, A. J., Clore, G. M., Gronenborn, A. M., Hardman, K. D., and Whitlow, M. (1992) *Biochemistry 31*, 10449−10457.
42. Gallagher, T., Alexander, P., Bryan, P., and Gilliland, G. L. (1994) *Biochemistry 33*, 4721−4729.
43. Gallagher, T., Alexander, P., Bryan, P., and Gilliland, G. L. (1994) *Biochemistry 33*, 10449−10457.
44. Konev, S. V. (1967) in *Fluorescence and Phosphorescence of Proteins and Nucleic Acids*, pp 30−33, Plenum Press, New York.
45. Chen, Y., and Barkley, M. D. (1998) *Biochemistry 37* (28), 9976−9982.
46. Feng, Z., Ha, J.-H., and Loh, S. N. (1999) *Biochemistry 38* (44), 14433−14439.
47. Ptitsyn, O. B., and Eizner, Y. E. (1959) *Z. Tekh. Fix. 23*, 1112−1134.
48. Blanco, F. J., and Serrano, L. (1995) *Eur. J. Biochem. 230* (2), 634−649.
49. Honda, Sh., Kobayashi, N., Munekata, E., and Uedaira, H. (1999) *Biochemistry 38*, 1203−1213.
50. Honda, Sh., Kobayashi, N., and Munekata, E. (2000) *J Mol. Biol. 295*, 269−278.
51. Frank, M. K., Clore, G. M., and Gronenborn, A. M. (1995) *Protein Sci. 4* (12), 2605−2615.

BI000345U